ACS central science

Research Article

http://pubs.acs.org/journal/acscii

Synthesis and Characterization of the Actinium Aquo Ion

Maryline G. Ferrier,[†] Benjamin W. Stein,[†] Enrique R. Batista,*[,†] John M. Berg,[†] Eva R. Birnbaum,[†] Jonathan W. Engle,[†,‡] Kevin D. John,[†] Stosh A. Kozimor,*[,†] Juan S. Lezama Pacheco,[§] and Lindsay N. Redman[†]

[†]Los Alamos National Laboratory, Los Alamos, New Mexico 87545, United States

[‡]University of Wisconsin, Madison, Wisconsin 53711, United States

[§]Stanford University, Stanford, California 94305, United States

Supporting Information

ABSTRACT: Metal aquo ions occupy central roles in all equilibria that define metal complexation in natural environments. These complexes are used to establish thermodynamic metrics (i.e., stability constants) for predicting metal binding, which are essential for defining critical parameters associated with aqueous speciation, metal chelation, *in vivo* transport, and so on. As such, establishing the fundamental chemistry of the actinium(III) aquo ion (Ac-aquo ion, $Ac(H_2O)_x^{3+}$) is critical for current efforts to develop ^{225}Ac [$t_{1/2}$ = 10.0(1) d] as a targeted anticancer therapeutic agent. However, given the limited amount of actinium available for study and its high radioactivity, many aspects of actinium chemistry remain poorly defined. We overcame these challenges using the longer-lived ^{227}Ac [$t_{1/2}$ = 21.772(3) y] isotope and report the first characterization of this fundamentally important Ac-aquo coordination complex. Our X-ray absorption fine structure study revealed 10.9 ± 0.5 water molecules directly coordinated to the Ac^{III} cation with an $Ac-O_{H2O}$ distance of 2.63(1) Å. This experimentally determined distance was consistent with molecular dynamics density functional theory results that showed (over the course of 8 ps) that Ac^{III} was coordinated by 9 water molecules with $Ac-O_{H2O}$ distances ranging from 2.61 to 2.76 Å. The data is presented in the context of other actinide(III) and lanthanide(III) aquo ions characterized by XAFS and highlights the uniqueness of the large Ac^{III} coordination numbers and long $Ac-O_{H2O}$ bond distances.

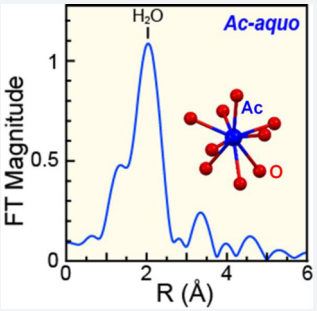

INTRODUCTION

Because metal aquo ions, $M(H_2O)_x^{n+}$, are both ubiquitous and chemically important, their structures and chemical properties serve as fundamental benchmarks in exploring trends across the periodic table. Characterization of aqueous speciation provides a foundation for advances throughout chemistry and biology. For example, understanding the chemistry of metal aquo ions is essential for solving technical problems relevant to biomedical applications, metal ions in the environment, extraction, food chemistry, and so on. In this sense, metal aquo ions occupy central roles in all chemical equilibria that define complexation properties of a metal by a particular ligand in aqueous media (eq 1).

$$M(H_2O)_x^{n+} \underset{-L}{\overset{+L}{\rightleftharpoons}} ML(H_2O)_{x-1}^{n+} \underset{-L}{\overset{+L}{\rightleftharpoons}} ML_2(H_2O)_{x-2}^{n+} \underset{-L}{\overset{+L}{\rightleftharpoons}} ML_3(H_2O)_{x-3}^{n+} \quad (1)$$

Historically, one of the first critical steps in characterizing the chemical behavior of any element involved establishing its aqueous coordination chemistry. These results provided a foundation for determining critical metrics (i.e., stability constants) and metal solution behavior (i.e., complexation, precipitation, etc.) that enabled predictive capability for metal binding affinity. These days, the aquo ion identities and behaviors for many elements are taken for granted, as they have been well established for decades.

Motivated by the recent global efforts to exploit radioactive decay from ^{225}Ac as a promising anticancer therapeutic agent, we set out to explore actinium's chemical binding properties in support of chelator design.[1,2] Unfortunately, an insufficient understanding of actinium coordination chemistry has considerably hindered development of an appropriate actinium chelator.[1] As an example, even something as fundamental as the actinium aquo ion, $Ac(H_2O)_x^{3+}$ (referred hereafter as Ac-aquo), remains poorly defined. Closing this gap is one of the first steps toward establishing thermodynamic data needed for predicting actinium behavior in biologically relevant media.

Gathering experimental information about actinium is difficult, primarily because all of its isotopes are highly radioactive. The most stable actinium isotopes—^{225}Ac and ^{227}Ac—have very short half-lives ($t_{1/2}$) of 10.0(1) d and 21.772(3) y,[3] respectively. Additionally, only very small quantities of these isotopes are available for research. As a result, many basic properties associated with actinium have yet to be defined. For instance, consider that the first actinium bond distance was not measured until 2016.[4] Perhaps the most well-defined aspect of actinium chelation chemistry is the realization that actinium's affinities for binding certain donor atoms are difficult to predict.[5] This deficiency, as well as the implications of

Received: November 18, 2016
Published: February 1, 2017

DOI: 10.1021/acscentsci.6b00356
ACS Cent. Sci. 2017, 3, 176−185

the large actinium ionic radius on chelation, severely hampers ligand design efforts for stabilizing actinium in targeted α-therapy applications.

Herein, we overcame the sample handling and spectroscopic obstacles associated with studying the actinium(III) ($5f^0$ $6d^0$) ion in aqueous media and report the first characterization of arguably the most fundamentally important actinium coordination complex, namely, the Ac-aquo ion, $Ac(H_2O)_x^{3+}$. In this study, we made use of X-ray absorption fine structure (XAFS) spectroscopy and molecular dynamics density functional theory (MD-DFT) calculations to evaluate actinium speciation in dilute triflic acid. These data were compared to previous actinium XAFS studies and presented in the context of what is currently understood for the other actinide(III) aquo ions.[4,6−16] Overall, the results highlight the uniqueness of the Ac^{III} ion, most notably in terms of the large coordination numbers and very long Ac−O_{H2O} bond distance.

RESULTS AND DISCUSSION

Sample Preparation. The synthesis of the Ac-aquo ion was inspired from methodology developed previously for other actinides (Scheme 1).[4,13,17−22] In general, the three step procedure involved (1) chemical and radiochemical purification to generate an ^{227}Ac stock solution, (2) preparation of the Ac-aquo ion, and (3) recovery of the valuable Ac^{III} reagent. The procedure started by chemically and radiochemically purifying a sample of actinium—recovered from a previous scientific campaign—using a combination of anion exchange (AG1-X8) and liquid/liquid extraction chromatography (branched DGA; Eichrom). In the course of our studies we found it important to add a cation exchange column to further purify Ac^{III} from organic contaminants that followed through the anion exchange and liquid/liquid extraction steps. Details associated with the first anion exchange and liquid/liquid extraction columns have been described previously.[4] In the cation exchange procedure, Ac^{III} dissolved in dilute nitric acid (HNO_3; 0.05 M) was loaded onto an AG50W-X8 resin. Under these conditions the resin bound Ac^{III} and organic contaminants were removed with copious HNO_3 (0.05 M) washing. Elution of the Ac^{III} in HNO_3 (6 M) provided a chemically pure stock solution that was suitable for subsequent chemical transformations. The overall purification procedure shown in Scheme 1 was attractive because it enabled recovery of Ac^{III} from numerous inorganic and organic contaminants. Additionally, the process reduced the dose rate by removing the radioactive daughters, namely, ^{227}Th and ^{223}Ra [$t_{1/2}$ = 18.68(9) d, 11.43(5) d, respectively].[4,17−23,5,24,25] Finally, this procedure provided a means to recycle the valuable and rare ^{227}Ac analyte for subsequent experimentation.

Scheme 1. Schematic Showing the Synthetic Methodology for Preparing the Ac-aquo Ion and Recovering Actinium from Previous Scientific Campaigns

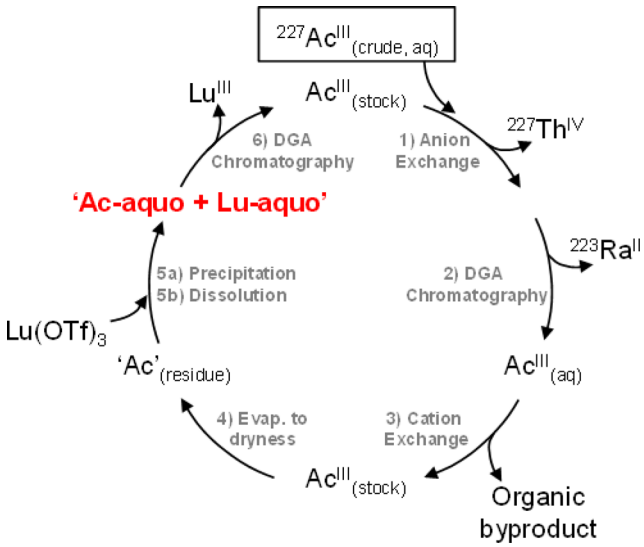

From the chemically and radiochemically purified actinium stock solution (described above) the Ac-aquo ion was prepared using a modification of the synthesis reported for the curium(III) aquo ion, $[Cm(H_2O)_9](CF_3SO_3)_3$.[13] This previously published $Cm(H_2O)_9^{3+}$ procedure involved precipitating Cm^{III} from aqueous solutions with sodium hydroxide (NaOH). The presumed curium(III) hydroxide was subsequently washed with water and dissolved in dilute triflic acid (HO_3SCF_3; 1.67 M). Unfortunately, in our laboratory, this hydroxide precipitation was not directly transferrable to our small actinium sample. For example, in the Cm^{III} study, there was sufficient mass (15 mg) to separate the curium(III) hydroxide precipitate from the supernate by centrifugation. In contrast, the Ac^{III} transformations were carried out on a microscale (only 30 μg). Hence, it was not possible to isolate the actinium(III) hydroxide—the most soluble f-element hydroxide[5]—using conventional separation methods from the aqueous solvent.

To overcome this technical challenge, we introduced stable lutetium as a macroscopic carrier to facilitate precipitation and isolation of actinium(III) hydroxide. Here, the purified Ac^{III} stock was heated under a stream of argon until the solvent evaporated. Care was taken to avoid bubble formation, splattering, and aerosolizing radioactive particles outside of the flask. After achieving a soft dryness, the residue was dissolved in water. Then, a macroscopic quantity of $Lu(CF_3SO_3)_3$ was added (0.5 mg) to the solution, and actinium(III) and lutetium(III) hydroxides were coprecipitated using NaOH (2 M). Centrifugation of the mixture generated a substantial pellet, from which the supernate was easily decanted and discarded. After washing the pellet and dissolving the solid in dilute triflic acid, a solution suitable for XAFS spectroscopy that contained macroscopic quantities of the Lu-aquo ion, $Lu(H_2O)_x^{3+}$,[26−31] with trace amounts of the Ac-aquo ion was obtained.

Several factors contributed to the success of this preparative method. First and foremost, the chemical behavior of Lu^{III} loosely mimics that of Ac^{III}, which ensured quantitative coprecipitation of the respective hydroxides. Additionally, there had to be a method to remove the Lu^{III} from Ac^{III} after the experiment, so that the precious actinium sample could be recycled for future studies. Consistent with many actinium/lanthanide separation studies,[17,5,24,25,32−38] we observed that liquid/liquid extraction chromatography (branched DGA; Eichrom) was effective for purifying Ac^{III} from Lu^{III}. As an example, "proof-of-principle" experiments using stable Lu^{III} (0.5 mg) spiked with a radioactive ^{173}Lu tracer [$t_{1/2}$ = 1.37(1) y; 5.8 kBq; 3.6×10^{11} atoms][3] and short-lived ^{225}Ac [$t_{1/2}$ = 10.0(1) d; 8.8 kBq; 1.1×10^{10} atoms] demonstrated feasibility.[3] These ^{173}Lu and ^{225}Ac isotopes were employed because their radioactive decay properties provided a convenient method for characterizing Lu^{III} and Ac^{III} separations using γ-spectroscopy. The representative chromatogram in Figure 1 shows that complete separation of ^{225}Ac from ^{173}Lu was achieved and that no cross contamination occurred in the representative ^{225}Ac and ^{173}Lu

DOI: 10.1021/acscentsci.6b00356
ACS Cent. Sci. 2017, 3, 176−185

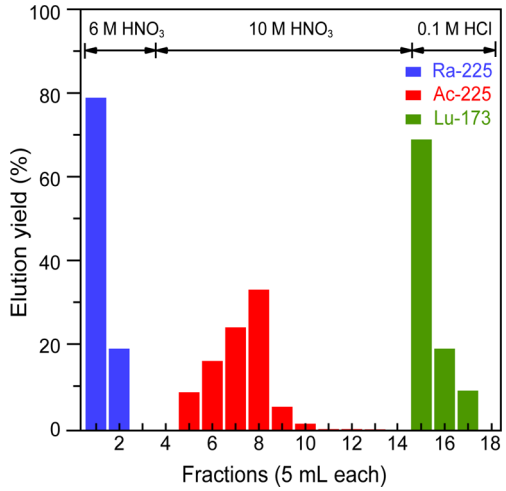

Figure 1. Elution profile of ^{225}Ra, ^{225}Ac, and ^{173}Lu separations using DGA (Eichrom) on a Bio-Rad column (1 mL of resin in 10 mL column).

fractions. Moreover, this procedure was successfully applied in recovering ^{227}Ac after the XAFS experiment. Although similar elution profiles were previously reported using trace quantities of actinium and lanthanides,[4,17,18,36,38−44] our separation demonstrated that the DGA process accommodated a large mass range. This spanned picogram (pg) to microgram (μg) quantities with successful separations both at the tracer level (^{225}Ac = 1.1×10^{10} atoms; ^{173}Lu = 3.6×10^{11} atoms) and using large masses (^{227}Ac = 7.4×10^{4} kBq, 7.4×10^{16} atoms, 2.8×10^{-5} g; stable Lu = 1.7×10^{18} atoms, 5.0×10^{-4} g).

Ac L_3-Edge XANES. To experimentally characterize Ac-aquo speciation, we exploited the element specific properties associated with X-ray absorption fine structure spectroscopy (XAFS). This spectroscopic approach has the crucial capability to probe low levels of actinium among large quantities of lutetium carrier. For instance, the Ac L_3-absorption edge is well separated in energy from the Lu K- and L-edges, as well as the corresponding X-ray emission lines used for fluorescence detection.[45] Figure 2 compares the background subtracted and normalized XANES spectrum from Ac-aquo (obtained in this study) with a spectrum of Ac^{III} dissolved in HCl (Ac^{III} in HCl; 11 M; Ac-HCl) from our previous work.[4] These two spectra are the only XANES measurements reported for actinium to date. The spectra were similar, each having a pronounced edge peak superimposed on an absorption threshold. From the perspective of the free ion, the edge feature has been crudely described as originating from electric-dipole allowed transitions from the actinide 2p-orbitals to unoccupied states that contain actinium 6d-character, i.e., $2p^6$ ... $5f^0$ $6d^0$ → $2p^5$ ... $5f^0$ $6d^1$.[46,47] The inflection point in the Ac-aquo spectrum was found at 15874.3 eV, as determined graphically where the second derivative of the data equaled zero. This value was 0.4 eV lower in energy than the analogous inflection point 15873.9 eV reported previously for Ac-HCl.[4] It was tempting to attribute this energy difference to electronic changes accompanying substitution of inner sphere Cl^{1-} ligands in Ac-HCl for H_2O ligands in Ac-aquo. However, given the uncertainty associated with actinide L-edge XANES inflection point determination, these energy differences were only marginally relevant statistically.

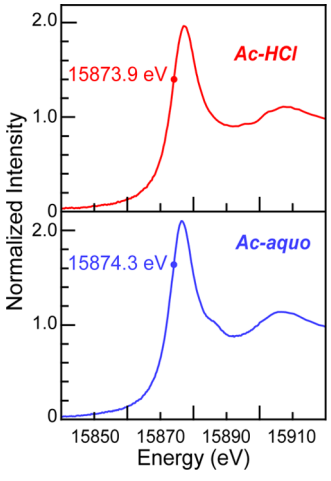

Figure 2. Room temperature background subtracted and normalized Ac^{III} L_3-edge XANES spectra obtained from Ac-aquo (HO_3SCF_3, 0.11 M; blue trace, bottom) and Ac-HCl (HCl, 11 M; red trace, top).

Ac-aquo MD-DFT. Before discussing the Ac L_3-edge EXAFS data, we found it instructive to first present results from the molecular dynamics density functional theory (MD-DFT) calculations. These computational results were used to guide the spectral interpretations by providing a glimpse into actinium species potentially present during the EXAFS experiment. In these calculations, the speciation of a single Ac^{III} ion with 64 H_2O molecules was modeled within a box that had dimensions of 12.54 Å × 12.45 Å × 12.68 Å. To keep the system neutral, the charge on the box was constrained to be uniformly −3. Prior to the simulation, the temperature was elevated (498 K) to randomize the box components. Next, the system was returned to 298 K and the molecular dynamics (MD) modeled for 8 ps. Results from the calculation are depicted graphically in Figure 3,

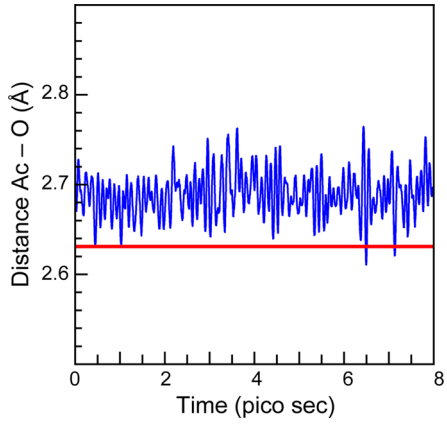

Figure 3. A comparison of the experimental Ac−O_{H2O} bond distance (red trace) determined by EXAFS spectroscopy and the calculated mean distance (blue trace) between Ac^{III} and water molecules within 3 Å from the actinium center during the 8 ps MD-DFT calculation.

where an averaged H_2O occupation was displayed as a function of the mean distance from the Ac^{III} ion over the course of the simulation. This plot showed a tight distribution of H_2O molecules at 2.689 ± 0.11 Å in the first actinium coordination sphere (Figure 4). Second and third shells of water molecules were subsequently observed near 5 and 7 Å, respectively, and linked to the first water shell through dynamic and intricate hydrogen bonding networks. However, over the course of the entire calculation only 9 H_2O molecules were ever observed in this first actinium coordination sphere. Attempts to add or

DOI: 10.1021/acscentsci.6b00356
ACS Cent. Sci. 2017, 3, 176−185

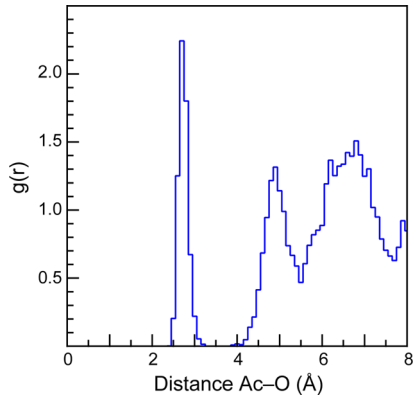

Figure 4. MD-DFT average radial distribution function of water molecules versus the calculated mean Ac−O_{H2O} distance during the 8 ps MD-DFT calculation.

subtract H_2O molecules failed, as a tenth H_2O molecule quickly disassociated and an eight coordinate $Ac(H_2O)_8^{3+}$ ion rapidly picked up an extra H_2O ligand.

Ac L_3-Edge EXAFS. Structural information for the Ac-aquo ion was experimentally determined from the $k^3\chi(k)$ EXAFS solution phase measurements shown in Figure 5 and Figure 6. In spite of the low analyte concentration, high quality data with a reasonable signal-to-noise ratio was obtained to approximately 8.5 k. As a result, the data confidently represented the actinium first coordination shell. Meanwhile, longer scattering pathways were obscured and not considered, i.e., the second water shell and multiple scattering pathways like Ac−H_2O···H_2O. The data was modeled using established methods based on the EXAFS equation,[48] where the coordination number (CN) and the bond length (R) variables were allowed to converge to reasonable values. Unfortunately, a reasonable model of the data could not be obtained when the Debye−Waller factor (σ^2) was a free variable. An unconstrained σ^2 model produced spectral fits with unreasonably large coordination numbers, or S_0^2 values >1 when coordination numbers were fixed. To overcome this challenge, σ^2 was constrained to the reasonable value of 0.009. As shown in the Supporting Information, this value was determined through extrapolation based on an anticipated linear relationship between σ^2 and the atomic number for the actinide aquo complexes (U to Cf)[6−16,49,50] listed in Table 1.

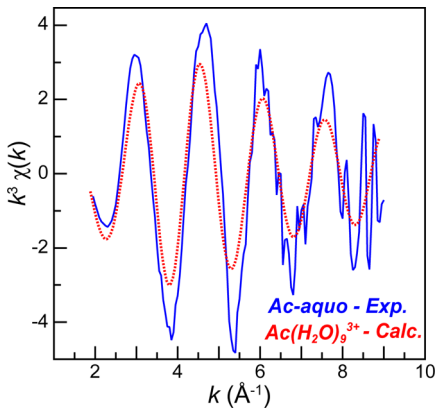

Figure 5. Room temperature solution-phase Ac^{III} L_3-edge EXAFS function $k^3\chi(k)$ from the Ac-aquo ion (HO_3SCF_3, 0.11 M) (solid blue trace) and a FEFF8 model for $Ac(H_2O)_9^{3+}$ (dashed red trace), whose coordinates were obtained from a single frame of the MD-DFT calculation.

To guide interpretations of the EXAFS data from Ac-aquo, we calculated (using FEFF8[51]) an EXAFS spectrum for a stable configuration of the actinium(III) nona-aquo trication, $Ac(H_2O)_9^{3+}$, based on atomic coordinates obtained from one "frame" of the MD-DFT calculations described above (see Figure 5). The experimental and calculated spectra were nearly superimposable, except at low k, owing to differences in the Debye−Waller factors (none were applied to the DFT model). Each spectrum was best described as having a single frequency whose amplitude methodically dampened with increased k. The frequencies were in good agreement, which suggested that the experimental Ac−O_{H2O} distances approximated those in the $Ac(H_2O)_9^{3+}$ model.

In the FEFF8 calculation (coordinates obtained from MD-DFT), the nine Ac−O_{H2O} scattering pathways ranged from 2.544 to 2.845 Å, spanning 0.301 Å. Given that the experimental data was of high quality between k of 2.6 and 8.5, the experimental resolution was calculated to be 0.266 Å ($\pi/2\Delta k$). Hence, we refrained from attempting to experimentally resolve multiple Ac−O_{H2O} bond distances within the first water shell. A high quality fit with low residual factors and a reduced chi-squared value were obtained using an "averaged" single H_2O shell, as displayed in Figure 6 for the $k^3\chi(k)$ data and its corresponding Fourier transform. In this model a shell of H_2O molecules was observed at a 2.63(1) Å distance (Table 1, Figure 6). This value

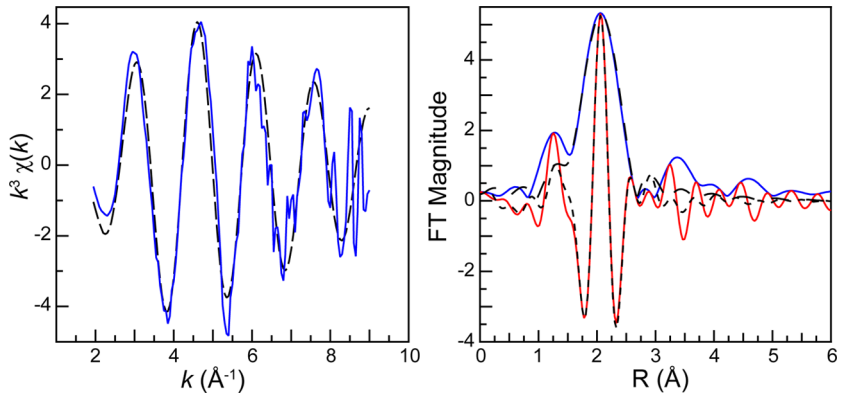

Figure 6. Left: The room temperature solution-phase Ac^{III} L_3-edge EXAFS function $k^3\chi(k)$ from the Ac-aquo ion (HO_3SCF_3, 0.11 M) (solid blue trace). Fit of the data is shown as a dashed black trace. Right: Fourier transform of k^3-EXAFS spectra from the Ac-aquo ion (HO_3SCF_3, 0.11 M; blue trace) and its real part shown as the red trace. Fits to the data have been provided as dashed black traces.

DOI: 10.1021/acscentsci.6b00356
ACS Cent. Sci. 2017, 3, 176−185

Table 1. Comparison of Lanthanide and Actinide +3 Aquo Ions Analyzed by EXAFS[a]

compound	metal soln concn	matrix	ionic radius (CN = 6)[63]	CN	R [Å]	σ^2 [Å^2]	ΔE_0 [eV]
Ac-aquo	**0.264 mM**	**0.11 M HO_3SCF_3**	**1.12**	**10.9 ± 0.5**	**2.63(1)**	**0.009**	**-3.9**
$La^{III}(H_2O)_y$[31]	0.2 M	pH 1 HO_3SCF_3	1.032	6.0 ± 0.5	2.560(9)	0.007(1)	
				3.0 ± 0.5	2.66(2)	0.0065(22)	
$La^{III}(H_2O)_y$[9]	2−3 M	0.25 M HCl	1.032	9.2 ± 0.37	2.54(3)	0.0090	−7.3
$La^{III}(H_2O)_y$[31]	0.2 M	pH 1 HO_3SCF_3	1.032	6.0 ± 1.0	2.50(4)	0.014(6)	
				3.0 ± 1.2	2.57(4)	0.009(7)	
$U^{III}(H_2O)_y$[6]	1−10 mM	pH 0 HCl	1.025	9.1 ± 0.6	2.52(1)	0.009(1)	12.8
U^{III}_{aq}[7]		1 M HCl	1.025	8.7 ± 0.9	2.56(1)	0.10(1)	2.1
$Np^{III}(H_2O)_y$[6]	0.5−2 mM	pH 0 HCl	1.01	10.0 ± 1.2	2.51(1)	0.009(1)	7.2
Np^{III}_{aq}[7]		1 M HCl	1.01	9.8 ± 0.9	2.52(1)	0.10(1)	3.8
Np^{III}_{aq}[8]	4.7 mM	1 M $HClO_4$	1.01	9.0 ± 1.0	2.48(2)		
$Pu^{III}(H_2O)_y$[49]	20 mM	0.01 M LiCl	1	10.2 ± 1.1	2.510(6)	0.010	−10.4
$Pu^{III}(H_2O)_y$[9]	10 mM	0.01 M LiCl	1	9.2 ± 0.33	2.510(6)	0.010	−10.4
$Pu^{III}(H_2O)_y$[6]	0.8−2 mM	pH 0 HCl	1	9.9 ± 0.3	2.49(1)	0.009(1)	7.0
Pu^{III}_{aq}[10]	0.01 mM	1 M $HClO_4$	1	8.6 ± 0.2	2.50(2)	0.0083	7.16
Pu^{III}_{aq}[7]		1 M HCl	1	9.9 ± 0.9	2.51(1)	0.10(1)	2.3
Pu^{III}_{aq}[50]			1	8−9	2.48		
$Nd^{III}(H_2O)_y$[9]	2−3 M	0.25 M HCl	0.983	9.5 ± 0.37	2.49(3)	0.0090	−8.2
$Nd^{III}(H_2O)_y$[52]		$HClO_4$	0.983	9.5	2.51	0.0091	
Am-aquo[4]	4.8 mM	0.11 M HO_3SCF_3	0.975	9.5 ± 0.87	2.48(1)	0.0088(9)	−4.71
$Am^{III}(H_2O)_y$[11]	1 mM	0.025 M $HClO_4$	0.975	8.3 ± 0.4	2.473(4)	0.0071(6)	−12.2
$Am^{III}(H_2O)_y$[9]	10 mM	0.25 M HCl	0.975	10.3 ± 0.33	2.480(6)	0.009	−8.7
$Am^{III}(H_2O)_y$[12]	7.9 mmol kg^{-1}	0.03 M $NaClO_4$ (pH 3.5)	0.975	9.0 ± 0.0	2.47(1)	0.0074(5)	7.2
Am^{III}_{aq}[7]		1 M HCl	0.975	9.5 ± 0.9	2.51(1)	0.10(1)	1.0
$Cm^{III}(H_2O)_y$[9]	10 mM	0.25 M HCl	0.97	10.2 ± 0.33	2.450(6)	0.009	−13.0
$Cm^{III}(H_2O)_y$[13]	0.523 M	1 M $HClO_4$	0.97	7.0 ± 0.4	2.469(7)	0.0071(8)	−2.0
$Bk^{III}(H_2O)_y$[14]	0.47 mM	1 M $HClO_4$ 1 M	0.96	9.0 ± 0.6	2.43(2)	0.009(2)	2.7
$Sm^{III}(H_2O)_y$[52]		$HClO_4$	0.958	9.3	2.45	0.0077	
Cf^{III}_{aq}[7]		1 M HCl	0.95	9.5 ± 0.9	2.44(1)	0.10(1)	2.5
$Cf^{III}(H_2O)_y$[15]	2.2 mM	0.1 M $HClO_4$	0.95	8.0 ± 0.0	2.42(1)	0.0077(1)	1.76
$Cf^{III}(H_2O)_y$[16]	1.67 M	1 M HCl	0.95	8.5 ± 1.5	2.42(2)	0.0095(1)	1.4
$Gd^{III}(H_2O)_y$[52]		$HClO_4$	0.938	7.6	2.41	0.0066	

[a]Data in bold are from this study, and data are presented in the order of decreasing ionic radius.[63]

was quite similar to the mean 2.66 ± 0.09 Å Ac−O distance for the static $Ac(H_2O)_9^{3+}$ structure obtained from the single "frame" of the MD-DFT simulation, which was used as the initial atomic coordinates guess in modeling the EXAFS data. We remind the reader of the MD-DFT results shown in Figure 3, where the average $Ac-O_{H2O}$ distances for the nine water molecules varied between ∼2.61 and ∼2.76 Å [mean 2.689 ± 0.11 Å] over an 8 ps dynamic simulation. These calculated values were similar to the experimentally determined distance. Additionally, this 2.63(1) Å experimental distance was quite similar to the only other reported $Ac-O_{H2O}$ distance, specifically the 2.59(3) Å distance determined recently by EXAFS from HCl solutions containing Ac^{III}, $AcCl_{3.2(1)}(H_2O)_{6.6(2)}$.[4] As these values are the only bond distances reported for actinium to date, their agreement is important in establishing confidence in the $Ac-O_{H2O}$ bond length being approximately 2.6 Å. Most notably, this $Ac^{III}-O_{H2O}$ distance was more than 0.1 Å longer than analogous distances in other actinide−aquo complexes, as determined by EXAFS analysis (see Table 1 and Figure 7).

The major difference between the EXAFS calculation from $Ac(H_2O)_9^{3+}$ and the experimental data was associated with wave amplitudes, which were larger in the experiment (Figure 5). This increase suggested that the experimental coordination number was greater than the calculation (coordination $number_{calc}$ = 9). The fit of the experimental data showed 10.9 ± 0.5 oxygen atoms in the inner Ac^{III} coordination sphere. The error with this coordination number is only associated with the data fitting model and does not encompass subjective decisions made during data processing (background subtraction, normalization, spline range, fitting range, Fourier transform range, choice of Debye−Waller factor, etc.). Having 10.9 ± 0.5 inner sphere water molecules seemed reasonable for the large Ac^{III} ion, especially because this value overlapped with coordination numbers determined by EXAFS for other +3 actinide and lanthanide

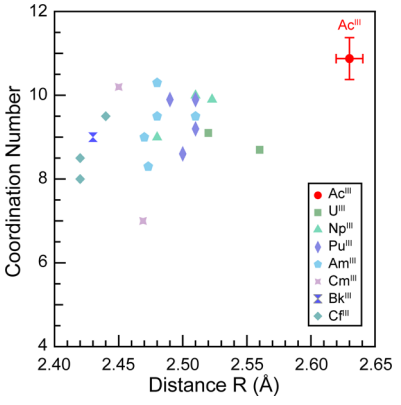

Figure 7. Coordination numbers and $An-O_{H2O}$ bond distances determined by EXAFS for the Ac-aquo ion and actinide(III) aquo ions previously reported.[6−16,49]

DOI: 10.1021/acscentsci.6b00356
ACS Cent. Sci. 2017, 3, 176−185

aquo ions (Table 1 and Figure 7). For the +3 actinides, these values ranged from 7.0 to 10.3 for U, Np, Pu, Am, Cm, Bk, and Cf[6−16,49,50] and averaged 9.3 ± 0.9. Similarly, for the +3 lanthanides, these values ranged from 7.6 to 9.5 for La, Nd, Sm, and Gd and averaged 9.0 ± 0.7.[9,31,52] We note that many of the coordination numbers determined by EXAFS for the actinide and lanthanide +3 aquo ions were larger than those observed by single crystal X-diffraction, where coordination numbers larger than 9 have yet to be reported.[13,26,30,53−62]

OUTLOOK

Herein, we characterized the Ac-aquo complex by Ac L_3-edge XAFS spectroscopy and MD-DFT calculations. Experimentally, we observed approximately 10.9 ± 0.5 water molecules in the inner actinium coordination sphere at an average distance of 2.63(1) Å. These results were in reasonable agreement with the MD-DFT results, which predicted exactly nine water molecules at a 2.689 ± 0.11 Å distance. The good agreement between experiment and theory is impressive when one accounts for the inherently large uncertainties typically associated with EXAFS coordination number determination alongside limitations associated with the GGA functionals and the difficulty in capturing key variables that influence speciation within the calculations. We anticipate that access to more experimental data, through studies like this, will reveal unique chemical and physical properties associated with the actinium element and enhance overall predictive capabilities in actinium chemistry. The characterization of the Ac-aquo ion presented here represents a fundamental benchmark in the development of actinium coordination chemistry. For example, with this data in hand, credible efforts to characterize actinium speciation in more relevant biological and natural media can proceed. In addition, characterization of the Ac-aquo ion will facilitate future efforts to study displacement of H_2O by chelating ligands.

While the Ac-aquo ion coordination number was slightly higher than the coordination numbers of the other actinide and lanthanide aquo ions, the incredibly long Ac−O_{H2O} distance exemplified how actinium is the largest +3 cation known (ionic radius: 1.12 Å[63]). While it remains unclear how actinium's unique size influences coordination numbers and preferences for binding certain donor atoms, the ion's size should be a major consideration when designing ligand architectures for actinium chelation. Hence, our current efforts are focused on characterizing the impact of actinium's large ionic radius on complexation by chelators relevant to biomimetic applications, i.e., DOTA, EDTA, HEHA, PEPA, DTPA, NOTA, etc.[2,64−69] These studies, in combination with the data reported here, will heavily influence our foray into developing new actinium chelators that support use of actinium in targeted α-therapy.

EXPERIMENTAL SECTION

General Consideration. ***CAUTION!*** *The ^{225}Ac, ^{227}Ac, and ^{173}Lu isotopes present serious health threats, due to their (and their daughters') α-, β-, and γ-radiation.* As such, this research was conducted in a radiological facility within certified fume hoods and monitored with appropriate α-, β-, and γ-particle detecting instruments. The ^{227}Ac isotope was supplied by the United States Department of Energy Office of Science Isotope Program in the Office of Nuclear Physics. The ^{173}Lu isotope was produced and purified at Los Alamos.[70] The ^{225}Ac isotope was purified from a clean ^{229}Th source, which had been achieved in the LANL isotope inventory many years ago.[71] Trifluoromethanesulfonic acid and sodium hydroxide were obtained commercially (Fisher Scientific). Water was purified to 18.2 MΩ/cm resistivity using Thermo-Scientific Barnstead Nanopure or Millipore Nanopure water purification systems. Resins used for separations—DOWEX AG1-X8 (BioRad; 100−200 mesh; Cl^{1-} form), branched DGA (Eichrom; 50 μm), and DOWEX AG50W-X8 (BioRad; 100−200 mesh; H^+ form)—were obtained commercially, suspended in water, and the fines were decanted prior to use. Separations were characterized using γ-spectroscopy using an EG&G Ortec model GMX-35200-S HPGe detector system in combination with a Camberra model 35-Plus multichannel analyzer associated with Gamma Vision software.

Ac^{III} Purification. Actinium was radiochemically and chemically purified as follows. A crude solution containing Ac^{III} in nitric acid, HNO_3 (~10 mL; 8 M), was loaded onto a Biorad column (10 mL) filled with DOWEX AG1-X8 (1 mL; BioRad; 100−200 mesh; Cl^{1-} form) that had been conditioned prior with H_2O (3 × 5 mL), HNO_3 (3 × 5 mL; 8 M), H_2O (3 × 5 mL), and HNO_3 (3 × 5 mL; 8 M). The Ac^{III} and ^{223}Ra daughter (+2 oxidation state) passed directly through the column, while the ^{227}Th daughter (+4 oxidation state) was retained. This effluent was diluted with water so that the final HNO_3 concentration was 6 M. This Ac^{III} containing solution was then loaded onto a second Biorad column (10 mL) containing a DGA (1 mL; Eichrom) resin that had been conditioned with H_2O (3 × 10 mL) followed by HNO_3 (1 × 10 mL; 6 M). Under these conditions the Ra^{II} passed through the column while Ac^{III} was retained. The column was washed with HNO_3 (6 × 2 mL; 6 M). Subsequently Ac^{III} was eluted using HNO_3 (2 × 5 mL; 0.05 M). To remove any organic compounds that followed Ac^{III} through the DGA resin, the DGA column effluent was loaded directly onto a Biorad column (10 mL) containing DOWEX AG50W-X8 resin (1 mL) that had been conditioned with H_2O (3 × 10 mL) and HNO_3 (1 × 10 mL; 0.05 M). After washing of the column with copious amounts of HNO_3 (2 × 5 mL; 0.05 M), Ac^{III} was eluted with HNO_3 (2 × 8 mL; 6 M). The ^{227}Ac fractions were combined. Subsequently 5 mL of the solution was assayed by γ-spectroscopy. We note that when assaying ^{227}Ac there is a large uncertainty (>3%) associated with γ-spectroscopy results, as the ^{227}Ac γ-emission is complicated by low relative intensities (0.001−0.006% at energies higher than 100 keV). Hence, more rigorous evaluation of the actinium concentration was achieved using the Bateman equation and monitoring ingrowth of the ^{227}Ac daughters, namely ^{227}Th and ^{223}Ra.[72]

Synthesis of Ac-aquo. The radiochemically and chemically purified Ac^{III} stock solution described above was evaporated to a soft dryness in a conical shaped glass vial on a hot plate under a slow stream of argon. The resulting residue was dissolved in Millipore H_2O (0.200 mL). Subsequently, sodium hydroxide, NaOH (0.100 mL; 2 M) was added and the solution was capped and agitated. To ensure quantitative precipitation and effective separation of actinium hydroxide precipitate from the supernate, lutetium(III) tris-triflate, $Lu(O_3SCF_3)_3$ (0.5 mg in 0.010 mL), was added as a stable carrier. The solution was then centrifuged (3 min at 6000 rpm) and the supernate was removed from the fluffy solid. The solid was washed with NaOH (1 × 0.100 mL; 10 mM) and with Millipore H_2O (1 × 0.050 mL). The solid precipitate was then dissolved in trifluoromethanesulfonic acid (HO_3SCF_3; 0.5 mL; 0.11 M) and transferred to an XAFS holder. The holder was triply contained, which protected against release of radiological material during shipment and XAFS experiments, as described below.

DOI: 10.1021/acscentsci.6b00356
ACS Cent. Sci. 2017, 3, 176−185

Ac^{III} Separation from Lu^{III}. A solution containing Ac^{III} and Lu^{III} was evaporated to a soft dryness in a conical shaped glass vial on a hot plate under a slow stream of air. The resulting residue was dissolved in HNO_3 (3 × 2 mL; 8 M). The resulting solution was loaded onto a Biorad column (10 mL) filled with a DGA (1 mL; Eichrom; 50 μm) resin that had been conditioned with H_2O (3 × 10 mL) followed by HNO_3 (3 × 10 mL; 6 M). Under these conditions both Ac^{III} and Lu^{III} were retained on the resin. Actinium(III) was selectively eluted with HNO_3 (5 × 10 mL; 10 M). The ^{227}Ac fractions were combined. Then, the solution was evaporated in a conical shaped glass vial on a hot plate under a slow stream of argon to a soft dryness. The residue was subsequently dissolved in a minimal amount of HNO_3 (8 M).

XAFS Measurements. The Ac L_3-edge XAFS measurements were made on samples loaded into XAFS cells that were triply contained. The XAFS holder consisted of a plastic body with a 2 mm well equipped with a set of Teflon windows (1 mil) and a Kapton window (1 mil). Solutions were introduced into the holder through an injection hole sealed with a Teflon gasket that was held in place by an aluminum plate. The sample cell holder was then transferred into the secondary and the tertiary container, which are best described as a set of nested aluminum holders equipped with Kapton windows (2 mil).

The XANES and EXAFS were measured at the Stanford Synchrotron Radiation Lightsource (SSRL) under dedicated operating conditions (3.0 GeV, 5%, 500 mA) on end station 11-2. This beamline was equipped with a 26-pole and a 2.0 T wiggler. Using a liquid nitrogen cooled double-crystal Si[220] ($\Phi = 0°$) monochromator and employing collimating and focusing mirrors, a single energy was selected from the incident white beam. Although the crystals were run fully tuned, higher harmonics from the monochromatic light were removed using a 370 mm Rh coated harmonic rejection mirror. The Rh coating was 50 nm with 20 nm seed coating, and the substrate was Zerodur. Vertical acceptance was controlled by slits positioned before the monochromator. The harmonic rejection cutoff was set by the mirror angle, thereby controlling which photons experience total external reflection. The samples were attached to the beamline 11-2 XAFS rail. The rail was equipped with three ionization chambers through which nitrogen gas was continually flowed. One chamber was positioned before the sample holder, to monitor the incident radiation (I_0, 10 cm). The second chamber was positioned after the sample holder, such that sample transmission (I_1, 30 cm) could be evaluated against I_0, while a third chamber (I_2, 30 cm) was positioned downstream from I_1 so that the XANES of a calibration foil could be measured in situ during the XAFS experiments against I_1. Actinium solution samples were measured in fluorescence mode using a solid-state 100-element Ge detector against the incident radiation (I_0). The 100-element Ge detector was windowed on the Ac Lα emission line (12.652 keV). Low energy contributions to the fluorescence signal were removed using a bromine filter (3 path lengths). Prior to conducting the measurements, dead time correction experiments were performed at approximately 400 eV above the element edge of the filter. The dead time correction curve corresponds to the plot of the windowed counts of the emission line of interest versus the total of incoming counts in the solid-state detector. This procedure was performed on a Se filter.

XAFS Data Analysis. Data manipulation and analysis was conducted as previously described.[4,48] First the data were dead time corrected and calibrated to the energy of the first inflection point of a rubidium(II) chloride, RbCl, pellet, diluted with boron nitride, BN, to a 1 absorption length thickness. The energy for the first inflection point for RbCl was determined in comparison to the Bi L_{II}-edge of a bismuth foil (15711 eV) to be 15874.3 eV. The energy of the calibration pellet was monitored before and after each Ac L_3-edge measurement. No energy drift during the experiment time was observed. The XAFS data were analyzed by fitting a line to the pre-edge region, which removed the background from experimental data in the spectra. Then a second to third order polynomial fitting was chosen for the postedge region. The difference between pre- and postedge lines was set to unity at the first inflection point, normalizing the absorption jump to 1.0. Samples were measured for several hours resulting in the collection of 31 scans. Fittings using Athena and Artemis[73] were performed using atomic coordinates from the MD-DFT calculations (see below) and FEFF8 calculations.[51] The spectra were fit using only single scattering paths obtained from FEFF8. The adjustments of spectra were performed in $2.6 < k < 8.5$ Å^{-1} and $1.25 < R < 3$ Å. For the fitting procedure, the coordination number (CN) and distance (R) variables were allowed to vary. In generating the model, the Debye−Waller factor (σ^2) was fixed to 0.009, which was extrapolated from the anticipated linear relationship between σ^2 and the atomic number anticipated for U−Cf aquo complexes (see the Supporting Information). A single value of energy shift (ΔE_0) was used for all scattering paths. The amplitude reduction factor (S_0^2) was set at 0.9 based on initial fits. Results were compared to data published previously for actinium in concentrated HCl (Ac-HCl).[4]

MD-DFT Calculations. The Born−Oppenheimer molecular dynamics (MD) simulations in the Helmholtz ensemble (NVT) were performed using the computer code VASP (Vienna Ab-initio Simulations Package)[74] version 5.35. In this code the forces on the ions are calculated from the electronic structure of the whole system computed using density functional theory at the generalized gradient approximation (GGA) level using the functional by Purdue−Burke−Enzerhof (PBE).[75] A simulation box of (12.54 × 12.45 × 12.68 Å^3) was used, including the metal ion (Ac^{3+}) surrounded by 64 water molecules while a uniform background charge of −3 was added to keep the neutrality of the simulation box. The basis set consists of an expansion into plane wave functions. Due to the large size of the simulation box the k-space representation included only the Γ point. The energy cutoff for the plane-wave expansion was set at 500 eV, and scalar relativistic effects were included using the PAW−PBE potentials.[76] Initially the metal ion and the closest neighboring molecules and counterions were kept frozen, and the solvent plus remaining counterion atoms were heated up to 498 K to be thermalized for 1 ps. After that a 1 ps run was done at 298 K with all the degrees of freedom released to thermalize the complex with the solvent. Finally 8 ps of data collection was performed where we monitored the solvent and ion dynamics.

■ ASSOCIATED CONTENT

Supporting Information

The Supporting Information is available free of charge on the ACS Publications website at DOI: 10.1021/acscentsci.6b00356.

A figure describing our determination for the Ac Debye−Waller factor (σ^2) (PDF)

■ AUTHOR INFORMATION

Corresponding Authors

*E-mail: erb@lanl.gov.

*E-mail: stosh@lanl.gov.

DOI: 10.1021/acscentsci.6b00356
ACS Cent. Sci. 2017, 3, 176−185

ORCID

Maryline G. Ferrier: 0000-0003-0081-279X

Notes

The authors declare no competing financial interest.

■ ACKNOWLEDGMENTS

We gratefully recognize the United States Department of Energy, Office of Science, Isotope Development and Production for Research and Application subprogram within Office of Nuclear Physics for their support in supplying the ^{227}Ac isotope. The work was funded under the LANL LDRD program (Berg, Birnbaum, Engle, Redman) and work under the Heavy Element Chemistry Program by the Division of Chemical Sciences, Geosciences, and Biosciences, Office of Basic Energy Sciences, U.S. Department of Energy and the U.S. Department of Energy (Batista, Kozimor). Portions of this work were supported by postdoctoral Fellowships from the Glenn T. Seaborg Institute (Ferrier, Stein). Los Alamos National Laboratory is operated by Los Alamos National Security, LLC, for the National Nuclear Security Administration of U.S. Department of Energy (Contract DE-AC52-06NA25396). Use of the Stanford Synchrotron Radiation Lightsource, SLAC National Accelerator Laboratory, was supported by the U.S. Department of Energy, Office of Science, Office of Basic Energy Sciences under Contract No. DE-AC02-76SF00515. The SSRL Structural Molecular Biology Program is supported by the DOE Office of Biological and Environmental Research, and by the National Institutes of Health, National Institute of General Medical Sciences (including P41GM103393). We thankfully acknowledge the computational resources for this project from the Environmental Molecular Science Laboratory of PNNL, in the cascade supercomputer. Some of the calculations were carried out with computational support of LANL's institutional computers, wolf cluster. The contents of this publication are solely the responsibility of the authors and do not necessarily represent the official views of NIGMS or NIH.

■ REFERENCES

(1) Kim, Y. S.; Brechbiel, M. W. An Overview of Targeted Alpha Therapy. *Tumor Biol.* **2012**, *33*, 573−590.

(2) Couturier, O.; Supiot, S.; Degraef-Mougin, M.; Faivre-Chauvet, A.; Carlier, T.; Chatal, J.-F.; Davodeau, F.; Cherel, M. Cancer Radioimmunotherapy with Alpha-Emitting Nuclides. *Eur. J. Nucl. Med. Mol. Imaging* **2005**, *32*, 601−614.

(3) Brookhaven National Laboratory. National Nuclear Data Center. http://www.nndc.bnl.gov/chart/.

(4) Ferrier, M. G.; Batista, E. R.; Berg, J. M.; Birnbaum, E. R.; Cross, J. N.; Engle, J. W.; La Pierre, H. S.; Kozimor, S. A.; Lezama Pacheco, J. S.; Stein, B. W.; Stieber, S. C. E.; Wilson, J. J. Spectroscopic and Computational Investigation of Actinium Coordination Chemistry. *Nat. Commun.* **2016**, *7*, 12312.

(5) Kirby, H. W.; Morss, L. R. Actinium. In *The Chemistry of the Actinide and Transactinide Elements*; Springer: Dordrecht, 2006; pp 18−51.

(6) Brendebach, B.; Banik, N. L.; Marquardt, C. M.; Rothe, J.; Denecke, M. A.; Geckeis, H. X-Ray Absorption Spectroscopic Study of Trivalent and Tetravalent Actinides in Solution at Varying pH Values. *Radiochim. Acta* **2009**, *97*, 701−708.

(7) David, F.; Fourest, B.; Hubert, S.; Le Du, J. F.; Revel, R.; Den Auwer, C.; Madic, C.; Morss, L. R.; Ionova, G.; Mikhalko, V.; Vokhmin, V.; Nikonov, M.; Berthet, J. C.; Ephritikhine, M. Aquo Ions of Some Trivalent Actinides: EXAFS Data and Thermodynamics Consequences. In *Speciation Techniques and Facilities for Radioactive Materials at Synchrotron Light Sources*; Edelstein, N., Nitshe, H., Reich, T., Eds.; Nuclear Energy Agency: Organization for Economic Co-Operation and development: Grenoble, France, 1998; pp 95−100.

(8) Antonio, M. R.; Soderholm, L.; Williams, C. W.; Blaudeau, J.-P.; Bursten, B. E. Neptunium Redox Speciation. *Radiochim. Acta* **2001**, *89*, 17−25.

(9) Allen, P. G.; Bucher, J. J.; Shuh, D. K.; Edelstein, N. M.; Craig, I. Coordination Chemistry of Trivalent Lanthanide and Actinide Ions in Dilute and Concentrated Chloride Solutions. *Inorg. Chem.* **2000**, *39*, 595−601.

(10) Kirsch, R.; Fellhauer, D.; Altmaier, M.; Neck, V.; Rossberg, A.; Fanghänel, T.; Charlet, L.; Scheinost, A. C. Oxidation State and Local Structure of Plutonium Reacted with Magnetite, Mackinawite, and Chukanovite. *Environ. Sci. Technol.* **2011**, *45*, 7267−7274.

(11) Stumpf, T.; Hennig, C.; Bauer, A.; Denecke, M. A.; Fanghänel, T. An EXAFS and TRLFS Study of the Sorption of Trivalent Actinides onto Smectite and Kaolinite. *Radiochim. Acta* **2004**, *92*, 133−138.

(12) Marques Fernandes, M.; Scheinost, A. C.; Baeyens, B. Sorption of Trivalent Lanthanides and Actinides onto Montmorillonite: Macroscopic, Thermodynamic and Structural Evidence for Ternary Hydroxo and Carbonato Surface Complexes on Multiple Sorption Sites. *Water Res.* **2016**, *99*, 74−82.

(13) Skanthakumar, S.; Antonio, M. R.; Wilson, R. E.; Soderholm, L. The Curium Aqua Ion. *Inorg. Chem.* **2007**, *46*, 3485−3491.

(14) Antonio, M. R.; Williams, C. W.; Soderholm, L. Berkelium Redox Speciation. *Radiochim. Acta* **2002**, *90*, 851−856.

(15) Galbis, E.; Hernández-Cobos, J.; Den Auwer, C.; Le Naour, C.; Guillaumont, D.; Simoni, E.; Pappalardo, R. R.; Sánchez Marcos, E. Solving the Hydration Structure of the Heaviest Actinide Aqua Ion Known: The californium(III) Case. *Angew. Chem.* **2010**, *122*, 3899−3903.

(16) Revel, R.; Den Auwer, C.; Madic, C.; David, F.; Fourest, B.; Hubert, S.; Le Du, J. F.; Morss, L. R. First Investigation on the L Edges of the ^{249}Cf Aquo Ion by X-Ray Absorption Spectroscopy. *Inorg. Chem.* **1999**, *38*, 4139−4141.

(17) Radchenko, V.; Engle, J. W.; Wilson, J. J.; Maassen, J. R.; Nortier, F. M.; Taylor, W. A.; Birnbaum, E. R.; Hudston, L. A.; John, K. D.; Fassbender, M. E. Application of Ion Exchange and Extraction Chromatography to the Separation of Actinium from Proton-Irradiated Thorium Metal for Analytical Purposes. *J. Chromatogr. A* **2015**, *1380*, 55−63.

(18) Horwitz, E. P.; McAlister, D. R.; Bond, A. H.; Barrans, R. E. J. Novel Extraction of Chromatographic Resins Based on Tetraalkyldiglycolamides: Characterization and Potential Applications. *Solvent Extr. Ion Exch.* **2005**, *23*, 319−344.

(19) Zielinska, B.; Apostolidis, C.; Bruchertseifer, F.; Morgenstern, A. An Improved Method for the Production of Ac-225/Bi-213 from Th-229 for Targeted Alpha Therapy. *Solvent Extr. Ion Exch.* **2007**, *25*, 339−349.

(20) Kotovskii, A. A.; Nerozin, N. A.; Prokof'ev, I. V.; Shapovalov, V. V.; Yakovshchits, Y. A.; Bolonkin, A. S.; Dunin, A. V. Isolation of Actinium-225 for Medical Purposes. *Radiochemistry* **2015**, *57*, 285−291.

(21) Boll, R. A.; Malkemus, D.; Mirzadeh, S. Production of Actinium-225 for Alpha Particle Mediated Radioimmunotherapy. *Appl. Radiat. Isot.* **2005**, *62*, 667−679.

(22) Alhassanieh, O.; Abdul-Hadi, A.; Ghafar, M.; Aba, A. Separation of Th, U, Pa, Ra and Ac from Natural Uranium and Thorium Series. *Appl. Radiat. Isot.* **1999**, *51*, 493−498.

(23) Aliev, R. A.; Ermolaev, S. V.; Vasiliev, A. N.; Ostapenko, V. S.; Lapshina, E. V.; Zhuikov, B. L.; Zakharov, N. V.; Pozdeev, V. V.; Kokhanyuk, V. M.; Myasoedov, B. F.; Kalmykov, S. N. Isolation of Medicine-Applicable Actinium-225 from Thorium Targets Irradiated by Medium- Energy Protons. *Solvent Extr. Ion Exch.* **2014**, *32*, 468−477.

(24) Hagemann, F. T. *The Chemistry of Actinium*. In *National Nuclear Energy Series, Manhattan Project Technical Section, Division 4: Plutonium Project 14A*; 1954; pp 14−44.

(25) Gmelin, L.; Alleluia, I. B.; Eberle, S. H.; Keller, C.; Kirby, H. W.; Munzel, H.; Seidel, A. *Gmelin Handbook of Inorganic Chemistry Ac Supplement Vol.1*, System num.; Kugler, H. K., Kelier, C., Eds.; Springer-Verlag: Berlin, Heidelberg, New York, 1981.

DOI: 10.1021/acscentsci.6b00356
ACS Cent. Sci. 2017, 3, 176−185

(26) Harrowfield, J. M.; Kepert, D. L.; Patrick, J. M.; White, A. H. Structure and Stereochemistry in "F-Block" Complexes of High Coordination Number. VIII The [M(unidentate)$_9$] System. Crystal Structures of [M(OH$_2$)$_9$] [CF$_3$S0$_3$]$_3$, M = La, Gd, Lu, Y. *Aust. J. Chem.* **1983**, *36*, 483−492.
(27) Chatterjee, A.; Maslen, E. N.; Watson, K. J. The Effect of the Lanthanoid Contraction on the nonaaqualanthanoid(III) Tris-(trifluoromethanesulfonates). *Acta Crystallogr., Sect. B: Struct. Sci.* **1988**, *44*, 381−386.
(28) Abbasi, A.; Lindqvist-Reis, P.; Eriksson, L.; Sandström, D.; Lidin, S.; Persson, I.; Sandström, M. Highly Hydrated Cations: Deficiency, Mobility, and Coordination of Water in Crystalline Nonahydrated scandium(III), yttrium(III), and lanthanoid(III) Trifluoromethanesulfonates. *Chem. - Eur. J.* **2005**, *11*, 4065−4077.
(29) Albertsson, J.; Elding, I. The Geometry of the Nonaaqualanthanoid(3+) Complex in the Solid Bromates and Ethyl Sulphates. *Acta Crystallogr., Sect. B: Struct. Crystallogr. Cryst. Chem.* **1977**, *33*, 1460−1469.
(30) Gerkin, R. E.; Reppart, W. J. The Structures of the Lanthanide Ethyl Sulfate Enneahydrates, M(C$_2$H$_5$SO$_4$)$_3$.9H$_2$O [M = La - Lu (except Pm)], at 171 K. *Acta Crystallogr., Sect. C: Cryst. Struct. Commun.* **1984**, *40*, 781−786.
(31) D'Angelo, P.; De Panfilis, S.; Filipponi, A.; Persson, I. High-Energy X-Ray Absorption Spectroscopy: A New Tool for Structural Investigations of Lanthanoids and Third-Row Transition Elements. *Chem. - Eur. J.* **2008**, *14*, 3045−3055.
(32) Kosynkin, V. D.; Moiseev, S. D.; Vdovichev, V. S. Cleaning Rare Earth Elements from Actinium. *J. Alloys Compd.* **1995**, *225*, 320−323.
(33) Sekine, T.; Koike, Y.; Hasegawa, Y. Studies of Actinium(III) in Various Solutions. II. Distribution Behavior of Lanthanum(III) and Actinium(III) in Some Chelate Extraction Systems. *Bull. Chem. Soc. Jpn.* **1969**, *42*, 432−436.
(34) Danon, J. Anion-Exchange Studies with Actinium and Lanthanides in Nitrate Solutions. *J. Inorg. Nucl. Chem.* **1958**, *7*, 422−424.
(35) Filosofov, D. V.; Lebedev, N. a.; Radchenko, V.; Rakhimov, A. V.; Happel, S.; Roesch, F. Behavior of Actinium, Alkaline, and Rare Earth Elements in Sr-Resin/Mineral Acid Systems. *Solvent Extr. Ion Exch.* **2015**, *33*, 496−509.
(36) Horwitz, E. P.; McAlister, D. R.; Thakkar, A. H. Synergistic Enhancement of the Extraction of Trivalent Lanthanides and Actinides by Tetra-(N-Octyl)Diglycolamide from Chloride Media. *Solvent Extr. Ion Exch.* **2008**, *26*, 12−24.
(37) Horwitz, E. P.; Bloomquist, C. A. A. Chemical Separations for Super-Heavy Element Searches in Irradiated Uranium Targets. *J. Inorg. Nucl. Chem.* **1975**, *37*, 425−434.
(38) Ostapenko, V.; Vasiliev, A.; Lapshina, E.; Ermolaev, S.; Aliev, R.; Totskiy, Y.; Zhuikov, B.; Kalmykov, S. Extraction Chromatographic Behavior of Actinium and REE on DGA, Ln and TRU Resins in Nitric Acid Solutions. *J. Radioanal. Nucl. Chem.* **2015**, *306*, 707−711.
(39) Lumetta, G. J.; Gelis, A. V.; Carter, J. C.; Niver, C. M.; Smoot, M. R. The Actinide-Lanthanide Separation Concept. *Solvent Extr. Ion Exch.* **2014**, *32*, 333−347.
(40) Sasaki, Y.; Sugo, Y.; Morita, K.; Nash, K. L. The Effect of Alkyl Substituents on Actinide and Lanthanide Extraction by Diglycolamide Compounds. *Solvent Extr. Ion Exch.* **2015**, *33*, 625−641.
(41) Sasaki, Y.; Tsubata, Y.; Kitatsuji, Y.; Sugo, Y.; Morita, Y.; Kimura, T. Extraction Behavior of Metal Ions by TODGA, DOODA, MIDOA, and NTAamide Extractants from HNO$_3$ to N-Dodecane. *Solvent Extr. Ion Exch.* **2013**, *31*, 401−415.
(42) Pourmand, A.; Dauphas, N. Distribution Coefficients of 60 Elements on TODGA Resin: Application to Ca, Lu, Hf, U and Th Isotope Geochemistry. *Talanta* **2010**, *81*, 741−753.
(43) Ansari, S. A.; Pathak, P. N.; Husain, M.; Prasad, A. K.; Parmar, V. S.; Manchanda, V. K. Extraction Chromatographic Studies of Metal Ions Using N, N, N′, N′ -Tetraoctyl Diglycolamide as the Stationary Phase. *Talanta* **2006**, *68*, 1273−1280.
(44) Husain, M.; Ansari, S. A.; Mohapatra, P. K.; Gupta, R. K.; Parmar, V. S.; Manchanda, V. K. Extraction Chromatography of Lanthanides Using N, N, N′, N′-tetraoctyl Diglycolamide (TODGA) as the Stationary Phase. *Desalination* **2008**, *229*, 294−301.
(45) Thompson, A.; Attwood, D.; Gullikson, E.; Howells, M.; Kim, K.-J.; Kirz, J.; Kortright, J.; Lindau, I.; Pianetta, P.; Robinson, A.; Scofield, J.; Underwood, J.; Vaughan, D.; Williams, G.; Winick, H. *Center for X-Ray Optics and Advanced Light Source X-Ray Data Booklet*, 2nd ed.; Lawrence Berkeley National Laboratory, University of California: Berkeley, CA, 2001.
(46) Teo, B. K. *EXAFS: Basic Principles and Data Analysis*; Springer-Verlag: New York, Berlin, 1986.
(47) Stohr, J. *NEXAFS Spectroscopy*, 1st ed.; Springer-Verlag: Berlin, 1992.
(48) Calvin, S. *XAFS for Everyone*; CRC Press Tayor and Francis Group: Boca Raton, FL, 2013.
(49) Allen, P. G.; Bucher, J. J.; Shuh, D. K.; Edelstein, N. M.; Reich, T. Investigation of Aquo and Chloro Complexes of UO_2^{2+}, NpO_2^{+}, Np^{4+}, and Pu^{3+} by X-Ray Absorption Fine Structure Spectroscopy. *Inorg. Chem.* **1997**, *36*, 4676−4683.
(50) Conradson, S. D. Application of X-Ray Absorption Fine Structure Spectroscopy to Materials and Environmental Science. *Appl. Spectrosc.* **1998**, *52*, 252A−279A.
(51) Ankudinov, A.; Conradson, S.; Mustre de Leon, J.; Rehr, J. Relativistic XANES Calculations of Pu Hydrates. *Phys. Rev. B: Condens. Matter Mater. Phys.* **1998**, *57*, 7518−7525.
(52) Yamaguchi, T.; Nomura, M.; Wakita, H.; Ohtaki, H. An Extended X-Ray Absorption Fine Structure Study of Aqueous Rare Earth Perchlorate Solutions in Liquid and Glassy States. *J. Chem. Phys.* **1988**, *89*, 5153−5159.
(53) Glaser, J.; Johansson, G. Crystal Strcutures of the Isomorphous Perchlorate Hexahydrates of Some Trivalent Metal Ions (M = La, Tb, Er, Tl). *Acta Chem. Scand.* **1981**, *35a*, 639−644.
(54) Habenschuss, A.; Spedding, F. H. The Coordination (Hydration) of Rare Earth Ions in Aqueous Chloride Solutions from X Ray Diffraction. II. $LaCl_3$, $PrCl_3$, and $NdCl_3$. *J. Chem. Phys.* **1979**, *70*, 3758−3763.
(55) Habenschuss, A.; Spedding, F. H. The Coordination (Hydration) of Rare Earth Ions in Aqueous Chloride Solutions from X Ray Diffraction. III.$SmCl_3$, $EuCl_3$, and Series Behavior. *J. Chem. Phys.* **1980**, *73*, 442−450.
(56) Paiva Santos, C. O.; Castellano, E. E.; Machado, L. C.; Vicentini, G. Crystal Structures of Neodymium and Holmium Trifluoromethanesulfonate Enneahydrated. *Inorg. Chim. Acta* **1985**, *110*, 83−86.
(57) Helmholz, L. The Crystal Structure of Neodymium Bromate Enneahydrate, Nd(BrO$_3$)$_3$.9H$_2$O. *J. Am. Chem. Soc.* **1939**, *61*, 1544−1550.
(58) Berthet, J. C.; Lance, M.; Nierlich, M.; Ephritikhine, M. Synthesis of the Uranium Triflates U(OTf)$_3$ and U(OTf)$_4$ − Crystal Structure of [U(OTf)$_2$(OPPh$_3$)$_4$][OTf]. *Eur. J. Inorg. Chem.* **1999**, *1999*, 2005−2007.
(59) Natrajan, L.; Mazzanti, M.; Bezombes, J.-P.; Pecaut, J. Practical Synthetic Routes to Solvates of U(OTf)$_3$: X-Ray Crystal Structure of [U(OTf)$_3$(MeCN)$_3$]$_n$, a Unique U(III) Coordination Polymer. *Inorg. Chem.* **2005**, *44*, 6115−6121.
(60) Matonic, J. H.; Scott, B. L.; Neu, M. P. High-Yield Synthesis and Single-Crystal X-Ray Structure of a Plutonium(III) Aquo Complex: [Pu(H$_2$O)$_9$][CF$_3$SO$_3$]$_3$. *Inorg. Chem.* **2001**, *40*, 2638−2639.
(61) Lindqvist-Reis, P.; Apostolidis, C.; Rebizant, J.; Morgenstern, A.; Klenze, R.; Walter, O.; Fanghänel, T.; Haire, R. G. The Structures and Optical Spectra of Hydrated Transplutonium Ions in the Solid State and in Solution. *Angew. Chem., Int. Ed.* **2007**, *46*, 919−922.
(62) Apostolidis, C.; Schimmelpfennig, B.; Magnani, N.; Lindqvist-Reis, P.; Walter, O.; Sykora, R.; Morgenstern, A.; Colineau, E.; Caciuffo, R.; Klenze, R.; Haire, R. G.; Rebizant, J.; Bruchertseifer, F.; Fanghänel, T. [An(H$_2$O)$_9$](CF$_3$SO$_3$)$_3$ (An = U-Cm, Cf): Exploring Their Stability, Structural Chemistry, and Magnetic Behavior by Experiment and Theory. *Angew. Chem., Int. Ed.* **2010**, *49*, 6343−6347.
(63) Shannon, R. D. Revised Effective Ionic Radii and Systematic Studies of Interatomic Distances in Halides and Chalcogenides. *Acta*

DOI: 10.1021/acscentsci.6b00356
ACS Cent. Sci. 2017, 3, 176−185

Crystallogr., Sect. A: Cryst. Phys., Diffr., Theor. Gen. Crystallogr. **1976**, *32*, 751−767.
(64) Davis, I. A.; Glowienka, K. A.; Boll, R. A.; Deal, K. A.; Brechbiel, M. W.; Stabin, M.; Bochsler, P. N.; Mirzadeh, S.; Kennel, S. J. Comparison of ^{225}Actinium Chelates: Tissue Distribution and Radiotoxicity. *Nucl. Med. Biol.* **1999**, *26*, 581−589.
(65) Chappell, L. L.; Deal, K. A.; Dadachova, E.; Brechbiel, M. W. Synthesis, Conjugation, and Radiolabeling of a Novel Bifunctional Chelating Agent for ^{225}Ac Radioimmunotherapy Applications. *Bioconjugate Chem.* **2000**, *11*, 510−519.
(66) McDevitt, M. R.; Ma, D.; Lai, L. T.; Simon, J.; Borchardt, P.; Frank, R. K.; Wu, K.; Pellegrini, V.; Curcio, M. J.; Miederer, M.; Bander, N. H.; Scheinberg, D. A. Tumor Therapy with Targeted Atomic Nanogenerators. *Science* **2001**, *294*, 1537−1540.
(67) McDevitt, M. R.; Ma, D.; Simon, J.; Frank, R. K.; Scheinberg, D. A. Design and Synthesis of ^{225}Ac Radioimmunopharmaceuticals. *Appl. Radiat. Isot.* **2002**, *57*, 841−847.
(68) Deal, K. A.; Davis, I. A.; Mirzadeh, S.; Kennel, S. J.; Brechbiel, M. W. Improved in Vivo Stability of Actinium-225 Macrocyclic Complexes. *J. Med. Chem.* **1999**, *42*, 2988−2992.
(69) Wilbur, S. D. Chemical and Radiochemical Considerations for Radiolabelling with Alpha-Emitting Radionuclides. *Curr. Radiopharm.* **2011**, *4*, 214−247.
(70) Taylor, W. A.; Rundberg, R. S.; Bond, E. M.; Nortier, F. M.; Vieira, D. J. Production of a ^{173}Lu Target for Neutron Capture Cross Section Measurements. *J. Radioanal. Nucl. Chem.* **2009**, *282*, 391−394.
(71) Wilson, J. J.; Ferrier, M.; Radchenko, V.; Maassen, J. R.; Engle, J. W.; Batista, E. R.; Martin, R. L.; Nortier, F. M.; Fassbender, M. E.; John, K. D.; Birnbaum, E. R. Evaluation of Nitrogen-Rich Macrocyclic Ligands for the Chelation of Therapeutic Bismuth Radioisotopes. *Nucl. Med. Biol.* **2015**, *42*, 428−438.
(72) Bateman, H. The Solution of a System of Differential Equations Occuring in the Theory of Radioactive Transformations. *Proc. Cambridge Philos. Soc.* **1910**, *15*, 423−428.
(73) Ravel, B.; Newville, M. ATHENA, ARTEMIS, HEPHAESTUS: Data Analysis for X-Ray Absorption Spectroscopy Using IFEFFIT. *J. Synchrotron Radiat.* **2005**, *12*, 537−541.
(74) Kresse, G.; Hafner, J. Ab Initio Molecular Dynamics for Liquid Metals. *Phys. Rev. B: Condens. Matter Mater. Phys.* **1993**, *47*, 558−561.
(75) Perdew, J. P.; Burke, K.; Ernzerhof, M. Generalized Gradient Approximation Made Simple. *Phys. Rev. Lett.* **1996**, *77*, 3865−3868.
(76) Kresse, G.; Joubert, D. From Ultrasoft Pseudopotentials to the Projector Augmented-Wave Method. *Phys. Rev. B: Condens. Matter Mater. Phys.* **1999**, *59*, 1758−1775.

DOI: 10.1021/acscentsci.6b00356
ACS Cent. Sci. 2017, 3, 176−185